Contact
Volume 6: 1–8

DOI: 10.1177/25152564231215133
journals.sagepub.com/home/ctc

Erythroid Differentiation Dependent Interaction of VPS13A with XK at the Plasma Membrane of K562 Cells

Chase Amos[1,2], Peng Xu[1,2], and Pietro De Camilli[1,2]

Abstract

Mutations of the bridge-like lipid transport protein VPS13A and the lipid scramblase XK result in Chorea Acanthocytosis (ChAc) and McLeod syndrome (MLS), respectively, two similar conditions involving neurodegeneration and deformed erythrocytes (acanthocytes). VPS13A binds XK, suggesting a model in which VPS13A forms a lipid transport bridge between the endoplasmic reticulum (ER) and the plasma membrane (PM), where XK resides. However, studies of VPS13A in HeLa and COS7 cells showed that this protein localizes primarily at contacts of the ER with mitochondria. Overexpression of XK in these cells redistributed VPS13A to the biosynthetic XK pool in the ER but not to PM-localized XK. Colocalization of VPS13A with XK at the PM was only observed if overexpressed XK harbored mutations that disengaged its VPS13A-binding site from an intramolecular interaction. As the acanthocytosis phenotype of ChAc and MLS suggests a role of the two proteins in cells of the erythroid lineage, we explored their localization in K562 cells, which differentiate into erythroblasts upon hemin addition. When tagged VPS13A was overexpressed in hemin-treated K562 cells, robust formation of ER–PM contacts positive for VPS13A was observed and their formation was abolished in XK KO cells. ER–PM contacts positive for VPS13A were seldom observed in undifferentiated K562 cells, despite the presence of XK in these cells at concentrations similar to those observed after differentiation. These findings reveal that the interaction of VPS13A with XK at ER–PM contacts requires a permissive state which depends upon cell type and/or functional state of the cell.

Keywords

lipid transfer protein, endoplasmic reticulum, plasma membrane, membrane, contact

Introduction

Chorea-Acanthocytosis (ChAc) and McLeod syndrome (MLS) are two similar clinical conditions, collectively called neuroacanthocytosis, characterized by degeneration of the brain caudate nucleus, resulting in Huntington's disease-like neurological manifestations, and the presence of abnormal red blood cells (acanthocytes) (Jung et al., 2011). ChAc is due to recessive mutations in VPS13A (Rampoldi et al., 2001; Ueno et al., 2001), a repeating beta-groove motif bridge-like lipid transport protein localized at membrane contact sites involving the endoplasmic reticulum (ER; Kumar et al., 2018; Dziurdzik and Conibear, 2021; Leonzino et al., 2021; Levine, 2022; Hanna et al., 2023). MLS is due to recessive mutations in XK (Ho et al., 1994), a lipid scramblase localized in the plasma membrane (PM; Adlakha et al., 2022; Ryoden et al., 2022). Recent studies have shown that the two proteins interact (Urata et al., 2019; Park and Neiman, 2020) via the binding of the Pleckstrin homology (PH) domain of VPS13A to a β-strand hairpin in the second cytosolic loop of XK (Guillen-Samander et al., 2022; Park et al., 2022) (Figure 1). Moreover, studies of regulatory T cells have shown that lack of either protein results in a defect of externalization at the PM of PtdSer, a phospholipid normally concentrated in its cytoplasmic leaflet (Ryoden et al., 2022). This led to a putative model according to which VPS13A and XK are functional partners: VPS13A would deliver phospholipids including PtdSer from the ER to the PM, while XK would

[1]Departments of Neuroscience and of Cell Biology, Howard Hughes Medical Institute, Program in Cellular Neuroscience, Neurodegeneration and Repair, Yale University School of Medicine, New Haven, CT, USA
[2]Aligning Science Across Parkinson's (ASAP) Collaborative Research Network, Chevy Chase, MD, USA

Received August 3, 2023. Revised October 31, 2023. Accepted November 2, 2023.

Corresponding Author:
Pietro De Camilli, Departments of Neuroscience and of Cell Biology, Howard Hughes Medical Institute, Program in Cellular Neuroscience, Neurodegeneration and Repair, Yale University School of Medicine, New Haven, CT 06510, USA.
Email: pietro.decamilli@yale.edu

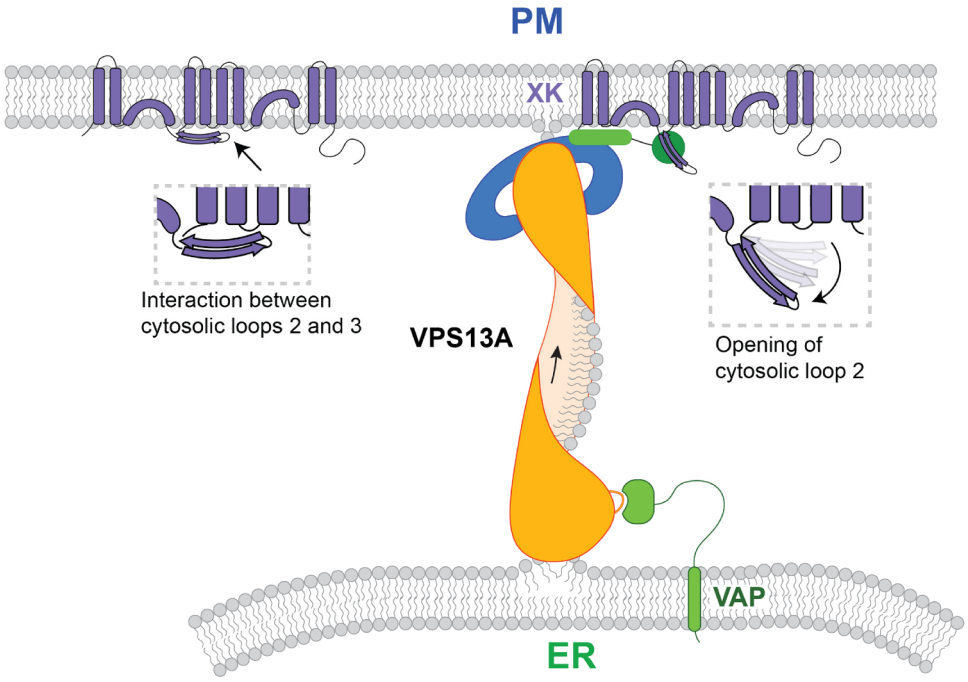

Figure 1. Model of VPS13A interaction with XK at the PM as proposed in Guillen-Samander et al. (2022). VPS13A binds VAP in the ER via an FFAT motif located in its N-terminal region, whereas its C-terminal PH domain binds the second cytosolic loop of XK. When explored in fibroblastic cells by exogenous expression of VPS13A and XK, the interaction of the two proteins at ER–PM contacts occurs only when an intramolecular interaction between loop 2 and loop 3 of XK (magnified in inset) is disrupted by point mutations (modified from Guillen-Samander et al., 2022).
PM = plasma membrane; ER = endoplasmic reticulum; PH = Pleckstrin homology.

collapse their asymmetric distribution between the two PM leaflets (Adlakha et al., 2022; Guillen-Samander et al., 2022; Park et al., 2022; Ryoden and Nagata, 2022).

However, imaging-based studies of tagged VPS13A expressed in commonly used fibroblastic cell lines (COS7 and HeLa cells) had failed to demonstrate enrichment of VPS13A at ER–PM contact sites, even upon co-expression of wild-type (WT) XK (Guillen-Samander et al., 2022). In these cells, VPS13A, when expressed alone, localizes primarily to ER-mitochondria contacts (Kumar et al., 2018; Guillen-Samander et al., 2022). This interaction occurs via the binding of its FFAT motif-containing N-terminal region to the ER protein VAP and of its C-terminal PH domain-containing region to a yet unknown binding site in the outer mitochondrial membrane (Kumar et al., 2018; Guillen-Samander et al., 2022). Co-expression of WT XK in these cells abolishes the localization of VPS13A to ER-mitochondria contacts, but does not result in its relocation to ER–PM contacts (Park and Neiman, 2020; Guillen-Samander et al., 2022). Under these conditions, VPS13A only colocalizes with the biosynthetic pool of XK in the ER, often in focal OSER-like accumulations, while no VPS13A can be found next to the PM pool of XK (Guillen-Samander et al., 2022). This relocation is due to the binding of the PH domain of VPS13A to ER-localized XK, which outcompetes its binding to mitochondria and likely results in an association of VPS13A with the ER mediated by both its N-terminal and C-terminal regions which bind VAP and XK, respectively (see Figure S3 in Guillen-Samander et al., 2022). While the PH domain of VPS13A can bind XK at the PM, transfected full-length VPS13A localizes with XK at the PM, where it also induces a prominent expansion of ER–PM contact sites, only if point mutations are introduced in XK to disrupt a predicted intramolecular interaction between its second and third cytosolic loop ($XK^{KKR>AAA}$ and $XK^{EYE>AAA}$) (Figure 1) (Guillen-Samander et al., 2022). These findings suggested that the formation of VPS13A and XK-dependent ER-–PM contacts is controlled by regulatory mechanisms that can be bypassed by mutant XK.

We considered the possibility that such mechanisms may be cell-type specific. As the acanthocytosis phenotype of ChAc and MLS suggests the special importance of VPS13A and XK in cells of the erythroid lineage, we explored the targeting of VPS13A in a model cell line with properties of such lineage. To this aim, we used K562 myelogenous leukemia cells, which undergo erythroid differentiation upon treatment with hemin, as shown by elevated hemoglobin content and erythroid lineage-specific transcriptional changes (Baliga et al., 1993; Huo et al., 2006),

including the initial induction of mitophagy as part of organelle clearance (Zhang et al., 2009; Fader et al., 2016). In these cells, we find that, after hemin-induced differentiation, VPS13A is present at ER–PM contacts and that this localization is dependent on endogenous XK, validating the hypothesis that they function together in a disease-relevant cell lineage.

Results

We first investigated the localization of VPS13A in undifferentiated K562 cells. As available antibodies do not detect endogenous VPS13A by immunofluorescence, we expressed a previously developed plasmid harboring an internal Halo tag, VPS13A^Halo (Kumar et al., 2018; Guillen-Samander et al., 2022). Similarly to what we had observed in HeLa and COS7 cells, this protein primarily localized at mitochondria, although in a pattern not precisely overlapping with the entire mitochondrial surface, as expected for a selective localization at ER-mitochondria contacts (Figure 2A). In HeLa and COS7 cells, VPS13A^Halo also localizes at ER–lipid droplet contacts, but no lipid droplets were present in our K562 cells. Next, we investigated the localization of VPS13A after hemin-induced differentiation. Consistent with previous reports (Baliga et al., 1993), incubation of cells in the presence of hemin for two days induced expression of hemoglobin with variable efficiency, as detected by a diaminobenzidine-based cytochemical reaction, confirming differentiation toward the erythroid lineage (Supplemental Figure S1). In striking contrast to what we had observed in undifferentiated cells, expression of VPS13A^Halo in hemin-treated cells resulted in its localization not only at mitochondria but also at the PM in a large fraction of the cells (Figure 2A–2D). This localization had the expected appearance of ER–PM contacts, as seen both in equatorial (positive segments along the PM) (Figure 2B) and basal planes (patches parallel to the substrate) (Figure 2C). Moreover, the expression of VPS13A^Halo and the ER marker GFP-Sec61β showed that cortical patches of VPS13A were connected to ER tubules (Figure 2E). The abundance and extent of these contacts were somewhat variables, most likely reflecting the variable efficiency of differentiation.

We next examined the impact of expressing exogenous XK on these localizations. As previously observed in COS7 cells (Guillen-Samander et al., 2022), co-expression of GFP-XK with VPS13A^Halo in non-differentiated K562 cells abolished the localization of VPS13A^Halo at mitochondria and resulted in its diffuse distribution throughout the cell, most likely reflecting colocalization with a pool of XK in the ER (Figure 3A). While a pool of GFP-XK^{WT} was observed at the PM in these cells, VPS13A^Halo did not colocalize with this pool. In contrast, in hemin-treated cells expressing GFP-XK^{WT}, VPS13A was additionally concentrated at PM patches (Figure 3A and 3C). Moreover, and in agreement with what we had observed in COS7 cells, co-expression of VPS13A^Halo with a GFP-XK construct harboring mutations in its second cytosolic loop (K105A/K106A/R107A, referred to as $XK^{KKR>AAA}$) which disrupts its interaction with the third loop (Guillen-Samander et al., 2022), accumulated at ER–PM contacts regardless of differentiation status (Figure 3B and 3C).

The most plausible interpretation of these findings is that the recruitment of VPS13A to the PM in differentiated cells is due to the hemin-dependent expression of endogenous XK. To address this possibility, we analyzed the expression of XK in K562 cells and we generated K562 cells lacking XK by Clustered Regularly Interspaced Short Palindromic Repeats (CRISPR)/CRISPR-associated protein 9 (Cas9) gene editing. Western blotting analysis of lysates surprisingly revealed that a band with the expected mobility of XK (Ryoden et al., 2022), and absent in XK KO K562 cells, was already present in non-differentiated cells (Figure 4A, lane 2). Total XK did not increase, and in fact showed a mild decrease after hemin (Figure 4A and 4B), potentially due to early stages of organelle clearance during differentiation toward erythrocytes. As a control, we found by western blotting that VPS13A was present at similar concentrations before and after hemin-induced differentiation (Figure 4C and 4D). However, the recruitment of VPS13A^Halo to the PM after hemin was abolished in XK KO cells, while the localization of VPS13A at mitochondria persisted, confirming the role of XK in its PM recruitment (Figure 4E to 4G). Note in Figure 4A the low expression of XK in COS7 cells relative to K562 cells, demonstrating cell type differences in the expression levels of XK. These findings demonstrate that the presence of endogenous XK is not sufficient to mediate VPS13A targeting to the PM, pointing to the occurrence of regulatory mechanisms that correlate with erythroid differentiation.

Discussion

Our findings prove that in erythroblast model cells, that is, cells of a lineage that undergo dysfunction upon loss of either VPS13A or XK, overexpressed VPS13A localizes at ER–PM contact sites dependently on XK. We also find that the presence of endogenous XK is not sufficient to result in their colocalization at ER–PM contacts. While levels of endogenous XK in K562 cells are similar before and after hemin-induced differentiation, such localization only largely occurs in hemin-differentiated cells. Thus, differentiation of K562 toward the erythrocyte lineage correlates with a cellular status that is permissive for the binding of full-length VPS13A to WT XK at the PM.

These mechanisms likely impact the intramolecular interaction between the second and third intracellular cytosolic loop of XK, as both in COS7 cells, where XK expression is comparatively low, and in undifferentiated K562 cells, which express robust levels of endogenous XK, this

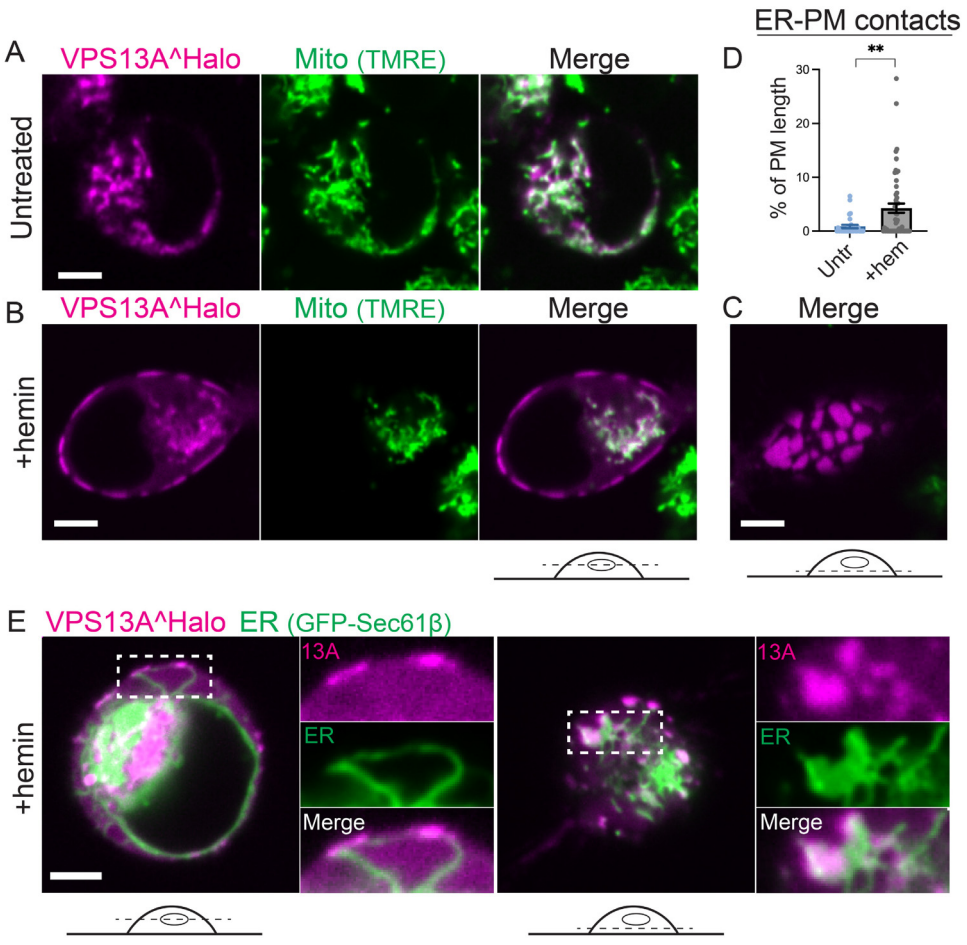

Figure 2. Overexpressed VPS13A is recruited to ER–PM contacts of K562 cells following their differentiation to the erythroid lineage by hemin. (A, B) Equatorial views of live K562 cells expressing VPS13A^Halo and untreated (A) or treated (B) with 30 μM hemin for 2 days and imaged after a brief incubation with TMRE, a live mitochondrial marker. Panel (C) shows the basal plane of the cell shown in the left panels revealing "en face" views of large ER–PM contacts. (D) Quantification of the fraction of PM profiles with VPS13A enrichment (D) ($n = 31$ untreated cells, 52 hemin-treated cells). (E) Equatorial (left) and basal (right) views of hemin-treated K562 cells co-expressing VPS13A^Halo and GFP-Sec61β. White rectangles outline areas shown at high magnification at the right of the main fields. $^{**}p < .01$. Scale bars indicate 5 μm. ER = endoplasmic reticulum; PM = plasma membrane; TMRE= tetramethylrhodamine ethyl ester.

intramolecular interaction must be disrupted to allow full-length VPS13A binding at the PM. Based on studies of the XK paralogue XKR8, the third intracellular loop of XK is likely to play a regulatory role in the scrambling activity of XK (Sakuragi et al., 2021). Thus, the involvement of this loop of XK in the regulation of VPS13A binding may reflect an interplay between VPS13A binding and the regulation of lipid scrambling. Why the binding of full-length VPS13A to endogenous XK at the PM, but not to XK in the ER, is affected by this erythroid differentiation-dependent switch in K562 cells, remains an open question.

In regulatory T cells, the partnership of VPS13A with XK is thought to be important for the externalization of PtdSer. Interestingly, *Drosophila* mutants lacking the VPS13A/VPS13C ortholog show a defect in the removal of cell corpses (Faber et al., 2020), a process that typically requires PtdSer exposure. Moreover, in erythroid differentiation, PtdSer externalization plays a role during the enucleation of erythroblasts when macrophages surround and then engulf the portion of the cell containing the nucleus (Moras et al., 2017). Thus, one could expect a defect in this process in cells lacking VPS13A or XK. However, so far, the main blood cell defect observed in ChAc and MLS is the presence of acanthocytes, that is, a defect of mature red cell morphology, rather than of red cell enucleation. In view of the scrambling activity of XK, it is of interest that acanthocytes can be the result of abnormal bilayer asymmetry leading to buckling of the membrane (Sheetz and Singer, 1974; Redman et al., 1989).

VPS13A is still present in the PMs of mature red cells, where its levels are drastically reduced in the absence of XK, suggesting that its interaction with XK stabilizes it (Urata et al., 2019). In fact, the lack of VPS13A in red cell membranes has been used to diagnose ChAc (Peikert et al., 2023). Thus, as

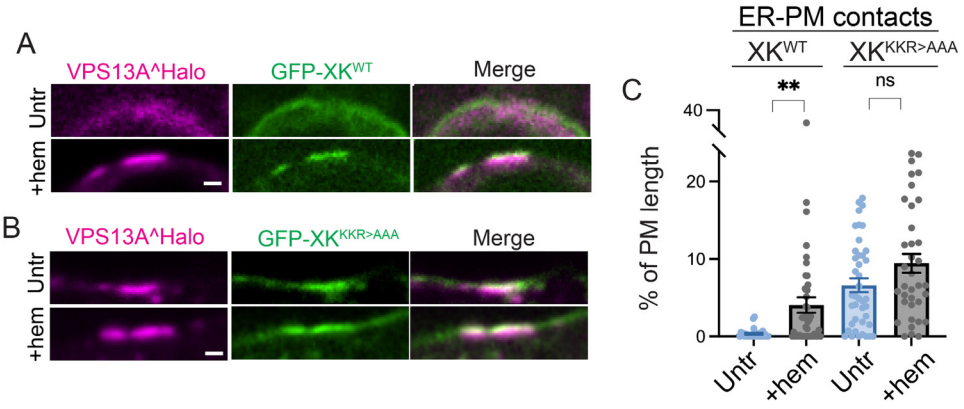

Figure 3. Expression of exogenous $XK^{KKR>AAA}$, but not of exogenous XK^{WT}, recruits VPS13A to ER–PM contacts also in undifferentiated K562 cells. Cortical regions of untreated or hemin-treated cells co-expressing GFP-XK^{WT} (A) or GFP-$XK^{KKR>AAA}$ (B) with VPS13A^Halo. PM-associated clusters of VPS13A^Halo and GFP-XK fluorescence reflects ER-PM contacts. (C) Quantification of the fraction of PM with VPS13A ($n = 26$ untreated XK^{WT} cells, 46 hemin-treated XK^{WT} cells, 41 untreated $XK^{KKR>AAA}$ cells, 36 hemin-treated $XK^{KKR>AAA}$ cells). $^{**}p < .01$, $^{n.s.}p > 0.05$. Scale bars indicate 1 μm.
ER = endoplasmic reticulum; PM = plasma membrane.

erythroblasts undergo full maturation to erythrocytes, VPS13A remains associated with XK despite the disappearance of the ER. A major outstanding open question is what may be the function of this protein which is thought to transport lipids from the ER to the PM, once the ER is no longer present. One possibility is that a regulatory function of VPS13A on the lipid scrambling activity of XK, irrespective of the lipid transport properties of VPS13A, may be preserved in mature red cells.

Methods

Plasmids

The plasmid encoding VPS13A^Halo (Kumar et al., 2018) (RRID:Addgene_118759) and GFP-XK (KKR>AAA mutant) (Guillen-Samander et al., 2022) was generated in our lab. GFP-XK was obtained from Genscript. GFP-Sec61β was a gift from T. Rapoport (Harvard University, Cambridge, MA) and mito-blue fluorescence protein (mito-BFP) from G. Voeltz (University of Colorado Boulder, Boulder) (RRID: Addgene_49151).

Cell Culture and Imaging

K562 cells (gift of Patrick Gallagher, Yale University) were cultured at 37 °C in 5% CO_2, in RPMI 1640 supplemented with fetal bovine serum, GlutaMAX, non-essential amino acids, and sodium pyruvate (Gibco). COS-7 cells (ATCC Cat No. CRL-1651, RRID:CVCL_0224) used for lysates were cultured in Dulbecco's modified eagle's medium (Gibco) with the same supplements. Prior to transfections, cells were maintained with penicillin/streptomycin (Gibco) and plasmocin (InvivoGen). For transfections, cells were plated on fibronectin (Sigma Aldrich) coated 35 mm imaging dishes (Mattek) in the same medium but without antibiotics and incubated overnight. Cells were then rinsed with a medium to remove non-adhering cells and cell debris, and a new medium was added containing the plasmids, FuGene 4K Transfection Reagent (Promega) as well as hemin in a subset of dishes. Hemin (Sigma Aldrich) dissolved in dimethyl sulfoxide was added at a final concentration of 30 μM. After overnight incubation with hemin and transfection reagents, the medium was replaced with a new medium containing the same factors for an additional overnight incubation. After two days following transfection and hemin treatment, cells were incubated with Halo ligands (gift of L. Lavis, Janelia Research Campus) for 90 min and rinsed with RPMI media. Immediately prior to imaging, live cells were stained with tetramethylrhodamine ethyl ester (TMRE; Cayman Chemical, TMRE Mitochondrial Membrane Potential Assay Kit). Imaging was performed at 37 °C, 5% CO_2 on an Andor Dragonfly (PlanApo 63× objective, 1.4 numerical aperture) microscope equipped with a Zyla cMOS camera. A Gaussian blur is applied to some of the images presented.

For diaminobenzidine staining, a final concentration of 0.2% 3,3′-diaminobenzidine tetrahydrochloride hydrate and 0.03% hydrogen peroxide (Sigma Aldrich) were combined in phosphate-buffered saline (PBS) immediately prior to staining. K562 cells on Mattek dishes were incubated with the diaminobenzidine/hydrogen peroxide mixture for 10 min at 37°C, 5% CO_2, washed with PBS, and the brightfield view was imaged using a ZOE Fluorescence Cell Imager (Bio-Rad).

For a detailed protocol for cell culture, transfection, and imaging, see https://dx.doi.org/10.17504/protocols.io.e6nvwdk4dlmk/v1.

Image Analysis

The fraction of PM occupied by VPS13A^Halo was quantified using FIJI (RRID:SCR_002285). Due to the close

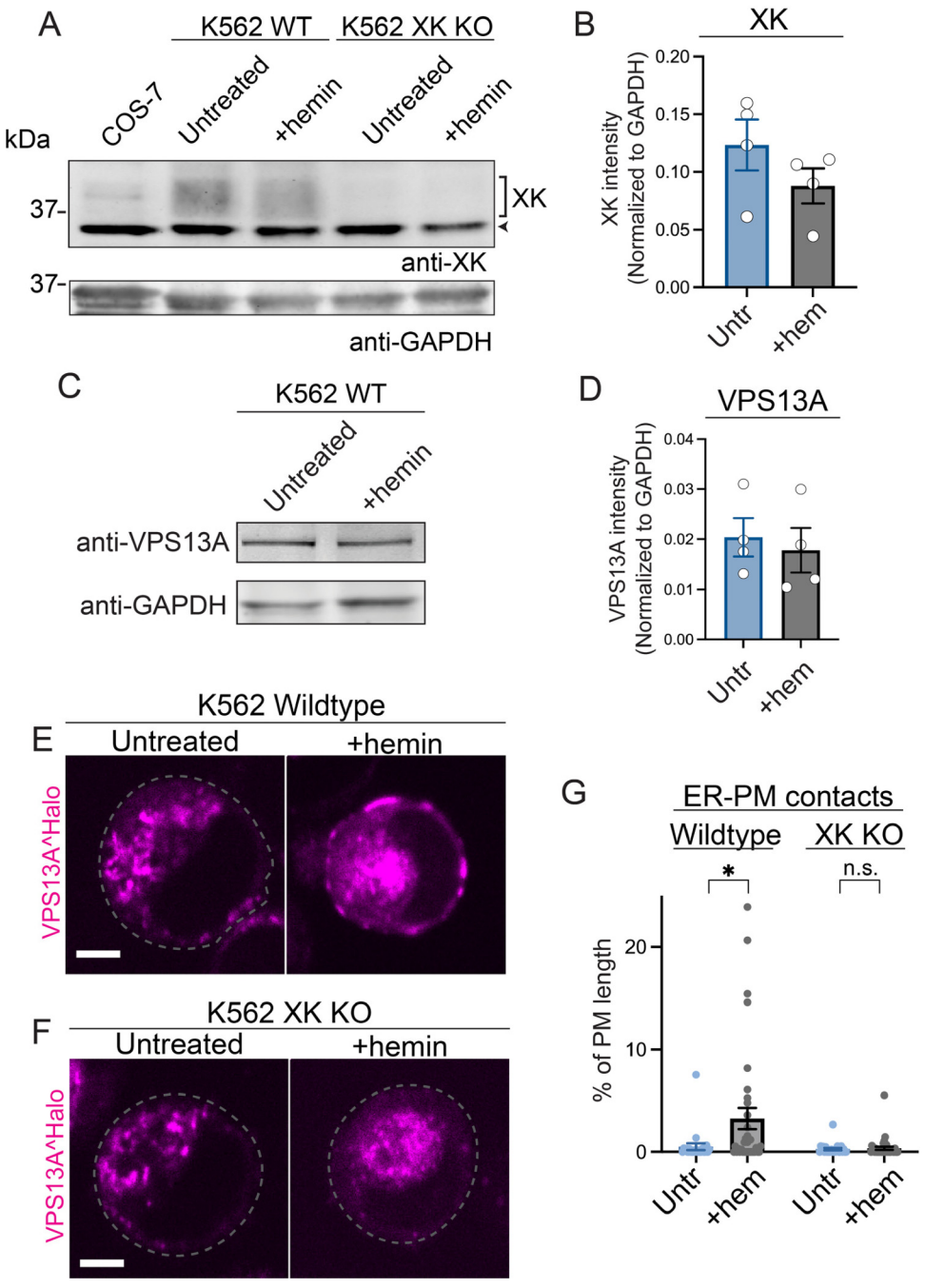

Figure 4. Recruitment of overexpressed VPS13A to the PM of erythroid cells depends on XK. Western blot of lysates from COS-7 cells and WT or XK KO K562 cells untreated or treated with hemin for 2 days (A), with quantification of XK intensities normalized to GAPDH input from western blots in (B) ($n = 4$ untreated, 4 hemin-treated lysates from WT K562 cells). An arrowhead indicates a non-specific band. Western blot of lysates from K562 cells before and after hemin-induced differentiation showing similar levels of VPS13A in the two conditions (C) with quantification of VPS13A intensities normalized to GAPDH (D) ($n = 4$ untreated, 4 hemin-treated lysates from WT K562 cells). (E–G) Wild-type (E) and XK KO (F) cells untreated or treated with hemin were transfected with VPS13A^Halo. Stippled lines indicate the cell profile in images where such profile is not visible. The fraction of the PM profiles occupied by VPS13A is shown in (G) ($n = 23$ WT untreated cells, 35 WT hemin-treated cells, 24 XK KO untreated cells, 36 XK KO hemin-treated cells). $^{*}p < 0.05$, $^{n.s.}p > 0.05$ by a unpaired Student's *t*-test (G). Scale bars indicate 5 μm. PM = plasma membrane; GAPDH = glyceraldehyde 3-phosphate dehydrogenase; WT = wild-type.

proximity of mitochondria to the cell edge, a negative mask generated from TMRE staining or mito-BFP overexpression was used to subtract the VPS13A^Halo signal originating from the mitochondria. The mitochondria-subtracted VPS13A channel was then thresholded to generate a binary mask of a signal at the PM. After tracing the cell edge, the

percentage of the PM length occupied by the binary VPS13A mask was measured.

For a detailed protocol for image analysis of PM contacts, see https://dx.doi.org/10.17504/protocols.io.n2bvj364plk5/v1.

Gene Editing

The knockout of XK was performed using a previously published CRISPR/Cas9 plasmid with a gRNA targeting exon 1 of XK (Guillen-Samander et al., 2022). The backbone was plasmid px459 (Addgene No. 62988) with the following XK gRNA sequence CCGTTGTCTCGGCCACGAACAGG (Guillen-Samander et al., 2022). K562 cells were transfected with this plasmid using the SF Cell Line 4D-Nucleofector kit and subsequently selected with 1 µg/mL puromycin prior to single-cell cloning. Sequencing of the gRNA-targeted exon 1 was performed by polymerase chain reaction amplification (Promega GoTaq polymerase) with 5′-GGTTTGGGGCT GGGCAT-3′ and 5′-AGGTGCAGCAGCAGTACG-3′ primers (Guillen-Samander et al., 2022) and cloning with the TOPO TA Cloning Kit (Invitrogen).

For a previously published detailed protocol for CRISPR/Cas9 editing of mammalian cells, see https://dx.doi.org/10.17504/protocols.io.5jyl85x89l2w/v1.

Western Blotting

K562 and COS-7 cells were lysed in 2% sodium dodecyl sulfate (SDS) and cleared by centrifugation at 13,300 r/min for 10 min after sonication. Lysates were mixed with a concentrated solution of SDS loading buffer to reach a final concentration of 50 mM Tris, pH 6.8, 2% SDS, 0.1% Bromophenol Blue, 10% glycerol, 1% beta-mercaptoethanol, heated for 10 min at 95°C, and loaded on 4% to 12% Tris-Glycine gels (Invitrogen). Gels were transferred to nitrocellulose membranes (Biorad) overnight at 30 V, 4°C. After blocking with 5% bovine serum albumin (BSA; Sigma Aldrich) in 1× Tris-buffered saline with Tween (TBS-T; Santa Cruz) for 1 h at room temperature, membranes were incubated overnight at 4 °C with anti-XK (Sigma-Aldrich Cat No. HPA019036, RRID:AB_1846286), anti-VPS13A (Novus Cat No. NBP1-85641, RRID:AB_11008734), or anti- glyceraldehyde 3-phosphate dehydrogenase (anti-GAPDH; EnCor Biotechnology Cat No. MCA-1D4, RRID: AB_2107599 in Figure 4A; Thermo Fisher Scientific Cat No. MA5-15738, RRID:AB_10977387 in Figure 4B to 4D) in 5% BSA in TBS-T. After three washes with TBS-T, membranes were incubated for 1 h at room temperature with LI-COR IRDye 680CW or 800CW secondary antibodies in 5% BSA in TBS-T, washed three times with TBS-T, and visualized using a Licor Odyssey Infrared Imager.

For a detailed protocol for western blotting, see https://dx.doi.org/10.17504/protocols.io.3byl4qb6zvo5/v1.

Statistical Analysis

Quantifications were analyzed using GraphPad Prism (RRID: SCR_002798). Unless otherwise indicated, all statistical analyses indicated are from an unpaired Student's *t*-test and graphs indicate mean ± SEM.

Acknowledgments

We thank Andres Guillén-Samander, Michael Hanna, Hanieh Falahati, Ben Johnson, and Sydney Cason for discussion. For open access, the author has applied a CC-BY-NC 4.0 public copyright license to the Author Accepted Manuscript (AAM) version arising from this submission.

Data Availability

All primary data associated with each figure have been deposited in the Zenodo repository and can be found using the following link: https://doi.org/10.5281/zenodo.10372977.

Declaration of Conflicting Interests

The authors declared no potential conflicts of interest with respect to the research, authorship, and/or publication of this article.

Funding

The authors disclosed receipt of the following financial support for the research, authorship, and/or publication of this article: This work was supported in part by NIH grants NS36251 and DA018343 and by the Parkinson Foundation (PF-RCE-1946). The study is funded by the joint efforts of The Michael J. Fox Foundation for Parkinson's Research (MJFF) and the Aligning Science Across Parkinson's (ASAP) initiative. MJFF administers the grant ASAP-000580 on behalf of ASAP and itself.

ORCID iDs

Chase Amos https://orcid.org/0000-0002-3176-9387
Peng Xu https://orcid.org/0000-0001-5197-9560
Pietro De Camilli https://orcid.org/0000-0001-9045-0723

Supplemental Material

Supplemental material for this article is available online.

References

Adlakha J, Hong Z, Li P, Reinisch KM (2022). Structural and biochemical insights into lipid transport by VPS13 proteins. J Cell Biol *221*, e202202030. doi: 10.1083/jcb.202202030

Baliga BS, Mankad M, Shah AK, Mankad VN (1993). Mechanism of differentiation of human erythroleukemic cell-line K-562 by hemin. Cell Proliferat *26*, 519–529. doi: 10.1111/j.1365-2184.1993.tb00030.x

Dziurdzik SK, Conibear E (2021). The Vps13 family of lipid transporters and its role at membrane contact sites. Int J Mol Sci *22*, 2905. doi: 10.3390/ijms22062905

Faber AIE, van der Zwaag M, Schepers H, Eggens-Meijer E, Kanon B, IJsebaart C, Kuipers J, Giepmans BG, Freire R, Grzeschik NA, et al. (2020). Vps13 is required for timely removal of nurse cell corpses. Development *147*, dev191759. doi: 10.1242/dev.191759

Fader CM, Salassa BN, Grosso RA, Vergara AN, Colombo MI (2016). Hemin induces mitophagy in a leukemic erythroblast cell line. Biol Cell *108*, 77–95. doi: 10.1111/boc.201500058

Guillen-Samander A, Wu YM, Pineda SS, Garcia FJ, Eisen JN, Leonzino M, Ugur B, Kellis M, Heiman M, De Camilli P (2022). A partnership between the lipid scramblase XK and the lipid transfer protein VPS13A at the plasma membrane. Proc Natl Acad Sci USA *119*, e2205425119. doi: 10.1073/pnas.2205425119.

Hanna M, Guillen-Samander A, De Camilli P (2023). RBG motif bridge-like lipid transport proteins: structure, functions, and open questions. Annu Rev Cell Dev Biol *39*, 409–434. doi: 10.1146/annurev-cellbio-120420-014634

Ho MF, Chelly J, Carter N, Danek A, Crocker P, Monaco AP (1994). Isolation of the gene for Mcleod syndrome that encodes a novel membrane-transport protein. Cell *77*, 869–880. doi: 10.1016/0092-8674(94)90136-8

Huo XF, Yu J, Peng H, Du ZW, Liu XL, Ma YN, Zhang X, Zhang Y, Zhao HL, Zhang JW (2006). Differential expression changes in K562 cells during the hemin-induced erythroid differentiation and the phorbol myristate acetate (PMA)-induced megakaryocytic differentiation. Mol Cell Biochem *292*, 155–167. doi: 10.1007/s11010-006-9229-0

Jung HH, Danek A, Walker RH (2011). Neuroacanthocytosis syndromes. Orphanet J Rare Dis *6*, 68. doi: 10.1186/1750-1172-6-68

Kumar N, Leonzino M, Hancock-Cerutti W, Horenkamp FA, Li PQ, Lees JA, Wheeler H, Reinisch KM, De Camilli P (2018). VPS13A and VPS13C are lipid transport proteins differentially localized at ER contact sites. J Cell Biol *217*, 3625–3639. doi: 10.1083/jcb.201807019

Leonzino M, Reinisch KM, De Camilli P (2021). Insights into VPS13 properties and function reveal a new mechanism of eukaryotic lipid transport. Biochim Biophys Acta Mol Cell Biol Lipids *1866*, 159003. doi: 10.1016/j.bbalip.2021.159003

Levine TP (2022). Sequence analysis and structural predictions of lipid transfer bridges in the repeating beta groove (RBG) superfamily reveal past and present domain variations affecting form, function and interactions of VPS13, ATG2, SHIP164, hobbit and tweek. Contact *5*, 251525642211343. doi: 10.1177/25152564221134328

Moras M, Lefevre SD, Ostuni MA (2017). From erythroblasts to mature red blood cells: organelle clearance in mammals. Front Physiol *8*, 1076. doi: 10.3389/Fphys.2017.01076

Park JS, Hu Y, Hollingsworth NM, Miltenberger-Miltenyi G, Neiman AM (2022). Interaction between VPS13A and the XK scramblase is important for VPS13A function in humans. J Cell Sci *135*, jcs260227. doi: 10.1242/jcs.260227

Park JS, Neiman AM (2020). XK is a partner for VPS13A: a molecular link between Chorea-Acanthocytosis and McLeod syndrome. Mol Biol Cell *31*, 2425–2436. doi: 10.1091/mbc.E19-08-0439-T

Peikert K, Dobson-Stone C, Rampoldi L, Miltenberger-Miltenyi G, Neiman A, De Camilli P, Hermann A, Walker RH, Monaco AP, Danek A (2023). VPS13A Disease. In: GeneReviews®. eds. MP Adam, GM Mirzaa, RA Pagon, SE Wallace, LJH Bean, KW Gripp, A Amemiya, Seattle, WA: University of Washington, Seattle.

Rampoldi L, Dobson-Stone C, Rubio JP, Danek A, Chalmers RM, Wood NW, Verellen C, Ferrer X, Malandrini A, Fabrizi GM, et al. (2001). A conserved sorting-associated protein is mutant in chorea-acanthocytosis. Nat Genet *28*, 119–120. doi: 10.1038/88821

Redman CM, Huima T, Robbins E, Lee S, Marsh WL (1989). Effect of phosphatidylserine on the shape of McLeod red-cell acanthocytes. Blood *74*, 1826–1835. doi: 10.1182/blood.V74.5.1826.1826

Ryoden Y, Nagata S (2022). The XK plasma membrane scramblase and the VPS13A cytosolic lipid transporter for ATP-induced cell death. Bioessays *44*, e2200106. doi: 10.1002/bies.202200106

Ryoden Y, Segawa K, Nagata S (2022). Requirement of Xk and Vps13a for the P2X7-mediated phospholipid scrambling and cell lysis in mouse T cells. Proc Natl Acad Sci USA *119*, e2119286119. doi: 10.1073/pnas.2119286119

Sakuragi T, Kanai R, Tsutsumi A, Narita H, Onishi E, Nishino K, Miyazaki T, Baba T, Kosako H, Nakagawa A, et al. (2021). The tertiary structure of the human Xkr8-Basigin complex that scrambles phospholipids at plasma membranes. Nat Struct Mol Biol *28*, 825–834. doi: 10.1038/s41594-021-00665-8

Sheetz MP, Singer SJ (1974). Biological membranes as bilayer couples. A molecular mechanism of drug-erythrocyte interactions. Proc Natl Acad Sci USA *71*, 4457–4461. doi: 10.1073/pnas.71.11.4457

Ueno S, Maruki Y, Nakamura M, Tomemori Y, Kamae K, Tanabe H, Yamashita Y, Matsuda S, Kaneko S, Sano A (2001). The gene encoding a newly discovered protein, chorein, is mutated in chorea-acanthocytosis. Nat Genet *28*, 121–122. doi: 10.1038/88825

Urata Y, Nakamura M, Sasaki N, Shiokawa N, Nishida Y, Arai K, Hiwatashi H, Yokoyama I, Narumi S, Terayama Y, et al. (2019). Novel pathogenic XK mutations in McLeod syndrome and interaction between XK protein and chorein. Neurology Genetics *5*, e328. doi: 10.1212/NXG.0000000000000328

Zhang J, Randall MS, Loyd MR, Dorsey FC, Kundu M, Cleveland JL, Ney PA (2009). Mitochondrial clearance is regulated by Atg7-dependent and -independent mechanisms during reticulocyte maturation. Blood *114*, 157–164. doi: 10.1182/blood-2008-04-151639